Self-healing epoxy coatings with microencapsulated ionic PDMS oligomers for corrosion protection based on supramolecular acid-base interactions

Oussama Boumezgane,[1] Raffaella Suriano,[1,] Michele Fedel,[2] Claudio Tonelli,[3] Flavio Deflorian,[2] Stefano Turri,[1]*

[1]Department of Chemistry, Materials and Chemical Engineering "Giulio Natta", Politecnico di Milano, Piazza Leonardo da Vinci 32, 20133 Milan, Italy

[2]Department of Industrial Engineering, University of Trento, via Sommarive, 9, 38123 Trento, Italy

[3]Solvay Specialty Polymers S.p.A., Viale Lombardia 20, Bollate (MI), Italy

*Corresponding author: raffaella.suriano@polimi.it

Abstract

To obtain a self-healing coating and improve the corrosion resistance of coated low-carbon steel surfaces, a commercial epoxy coating was modified by adding microcapsules composed of a poly(methyl methacrylate) shell and a core of ionic polydimethylsiloxane (PDMS) oligomers. The encapsulation of amino- and carboxylic acid-terminated PDMS was achieved by a solvent evaporation process after the emulsification of core and shell materials, dissolved in CH_2Cl_2, in a suitable colloidal solution. A high core loading of nearly 50% wt. was successfully obtained by carefully increasing the interfacial tension of oil-in-water emulsion before the solvent evaporation. The microcapsule morphology was evaluated by SEM and optical microscopy analyses, which showed a particle diameter range of 20-70 μm. The presence of ionic PDMS oligomers as core materials was demonstrated by FTIR spectroscopy and thermogravimetric analysis (TGA), which was also employed to determine the core loading. The newly prepared microcapsules were then incorporated into the matrix of a commercial two-component epoxy coating. Corrosion protection abilities were assessed by comparing samples coated with a standard epoxy coating modified with a 20% wt. of microcapsules and the pristine epoxy coating. The corrosion protection performance of the modified coating was evaluated through electrochemical impedance spectroscopy (EIS) tests and potential vs time measurements, which showed that the microcapsules in the coating matrix caused a beneficial increase in barrier properties of a scratched coating. The surface damage triggered the release of functional PDMS oligomers, leading to the formation of a supramolecular ionic network and providing self-healing abilities to the modified coating.

Keywords

Self-healing; smart coatings; microcapsules; supramolecular materials; electrochemical impedance spectroscopy (EIS); anti-corrosion

1. Introduction

The economic impact of corrosion of metallic structures in aggressive environments is a global industrial issue [1, 2]. A recent study has estimated that 15-35% of the costs of corrosion could be avoided [3]. One of the approaches used to prevent corrosion is the application of polymeric coatings on metallic structures [4]. The application of protective polymeric coatings that act as a barrier against corrosive species is the most common and cost-eff ective method of improving corrosion resistance behavior, and therefore the durability of metallic structures [5-7]. However, cracks can occur on the surface of coatings, which can disturb the protection process and in some cases could lead to a situation worse than the uncoated surface [8]. Different corrosion inhibitors have been introduced into coatings to protect metal substrates [9]. Moreover, self-healing materials as organic coatings have been proposed to extend metallic material lifetime against corrosion and recover its initial properties, after cracking due to the external environment or internal stresses [10]. Hence, in a self-healing coating, whenever scratch damage occurs or a crack initiates, healing occurs and protects the crack from propagation, decreasing the diffusion of oxygen, water, and ions down to the substrate [11].

Two different typologies of self-healing coatings can show an anti-corrosion effect: intrinsic and extrinsic self-healing coatings [12]. Intrinsic self-healing coatings are based on reversible reactions and interactions in the materials composed of functional chemical groups that can be rearranged by an external stimulus [13]. On the other hand, extrinsic self-healing coatings are activated by the release of self-healing agents from an encapsulating container after damage, intentionally embedded such as in micro- and nano-particles in an encapsulation process [14-16].

The encapsulation process consists of enclosing a well-defined material, which can be solid, liquid, or even gas in a thin shell of another material. A capsule is therefore a system that contains a core in a shell, consisting of a continuous, porous, or non-porous polymeric phase [17, 18]. In comparison to other strategies employed to obtain self-healing coatings, the encapsulation process presents the following advantages: i) polymers with any molecular structures can be potentially endowed with self-healing abilities by using healing agent-loaded capsules; ii) it is a well-established technology since its appearance in the 1950s [19, 20]; and iii) the microcapsules can be easily incorporated into a polymer carrier [21]. Different approaches are known in the state of art for the encapsulation of liquid and solid substances. Among these, there are the encapsulation via coacervation [22, 23], the in situ polymerization [24, 25], interfacial polymerization [26], the so-called Pickering emulsion templating [27-29] and solvent evaporation/extraction [30-32].

This work presents the encapsulation of amino- and carboxylic acid- terminated polydimethylsiloxane (PDMS) oligomers (Figure 1a) and the use of newly prepared microcapsules to provide self-healing anti-corrosive abilities to commercial epoxy coatings. In a previous study, amino-terminated PDMS oligomers are applied by dip-coating to impart self-cleaning properties to self-healable polyurethane coatings with self-healing abilities [33]. Many other works report the development of self-repairing coatings based on either the Diels-Alder chemistry [34] or the formation of sacrificial hydrogen bonds and dynamic imine bonds [35], starting from amino-terminated PDMS oligomers. Amino-terminated PDMS precursors are also employed to develop hydrophobic coatings with good corrosion resistance [36] and with anti-fouling performance [37]. In the present work, the PDMS oligomers are able, once mixed, to generate a supramolecular polymer network via acid-base interactions (Figure 1b, c, and d), which can repair the damage induced in coatings and therefore prevent corrosion [38]. Such an encapsulation process is not obvious for these oligomers due to their amphiphilic nature, which prevents the successful exploitation of usual oil-in-water encapsulation processes [39]. Moreover, the use of microcapsules loaded with functional ionic PDMS oligomers provides corrosion barrier properties even in successive damage events. The corrosion protection provided by the system presented in this work is therefore effective in longer immersion time than other self-healing systems based on non-reactive encapsulated healing agents [40].

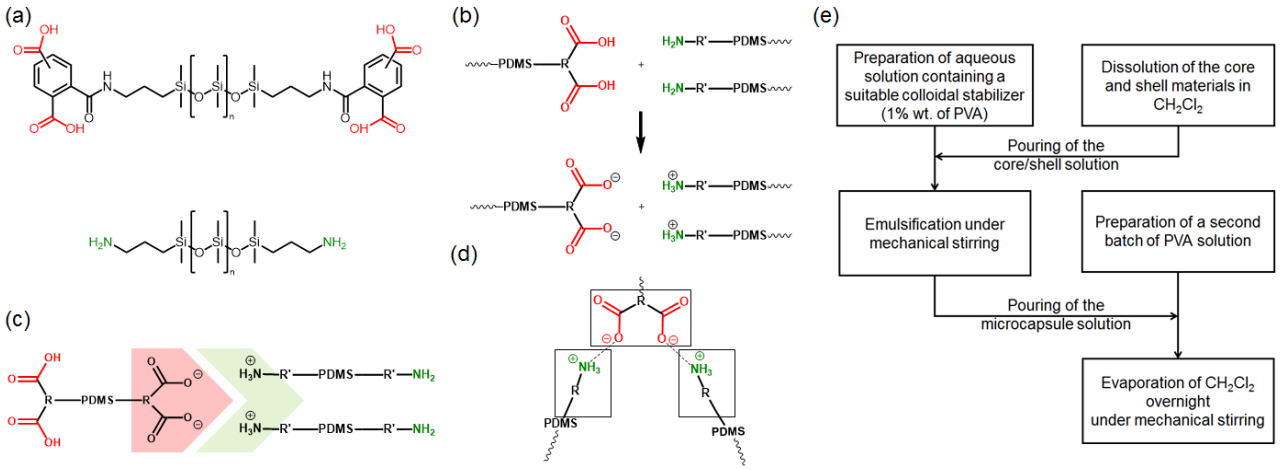

Figure 1. (a) Chemical structures of the amino- and carboxylic acid-terminated polydimethylsiloxane (PDMS); (b) and (c), schematic representation of the formation of ionic groups and acid-base interactions between the amino- and carboxylic acid-terminated PDMS; (d) scheme of the supramolecular polymer network, considering a theoretical 1:1 stoichiometry ratio between dicarboxylic/diamine units; and (e) procedure for the encapsulation of amino- and carboxylic acid-terminated PDMS.

2. Materials and methods

2.1 Materials

Aminopropyl-terminated polydimethylsiloxane, (PDMS-(2-NH_2)), and tetra-carboxylic acid terminated polydimethylsiloxane, PDMS-(4-COOH) were used as core materials. (PDMS-(2-NH_2)) was purchased by Gelest, Inc. (product code: DMS-A15) and it was characterized by a molecular weight of 3000 g/mol, a viscosity of 50-60 cSt at 25 °C, and two terminal amine groups. PDMS-(4-COOH) was synthesized and functionalized with four carboxylic acid groups and it was provided by Solvay Specialty Polymers S.p.A [41-44].

Poly(methyl methacrylate) (PMMA) with a molecular weight of 350000 Da, purchased from Sigma-Aldrich, was used as a shell material. Polyvinyl alcohol (PVA, hydrolyzed with a purity = 98-99%) with a molecular weight in the range [31000 ÷ 50000 g/mol] was purchased from Sigma-Aldrich. Dichloromethane, dodecane, and sodium chloride (NaCl) were also purchased from Sigma-Aldrich and used as received.

2.2 Encapsulation process

The procedure used is an encapsulation via solvent evaporation/extraction [21, 31, 32, 45]. The encapsulation procedure was carried out separately for the two core materials, (PDMS-(2-NH_2)) and PDMS-(4-COOH). Amine/carboxylic acid terminated PDMS (as core materials) and PMMA were dissolved in dichloromethane, used as a volatile solvent in the microencapsulation process. For the encapsulation of PDMS-(2-NH_2), the concentration of PMMA and the core material was nearly 14% wt., while the ratio between core and shell materials was equal to 3. For the encapsulation of PDMS-(4-COOH), the concentration of PMMA and the core material was nearly 13% wt., while the ratio between PDMS-(4-COOH), which was diluted with 33.3% wt. of dodecane with respect to the PDMS oligomer weight, and PMMA was equal to 2. Meanwhile, an aqueous solution containing 1% wt. of PVA, used as a polymeric emulsion stabilizer, and ≈ 3% wt. of NaCl was prepared. 250 ml of PVA solution were added to a beaker and mechanically stirred at nearly 700 rpm, for around 20 min. Then, the core/PMMA solution was added to the PVA solution at a rotation speed of 600 rpm for nearly 1 h for the emulsification step. Afterward, the emulsion was poured into 125 ml of PVA solution and kept under a fume hood overnight for the solvent evaporation step. The obtained microcapsules were filtrated and washed with distilled water and hexane to remove the residual non-encapsulated core materials and let dry under vacuum at 50 °C. The conditions used for the procedure of encapsulation, for both amine and carboxylic acid-functionalized polydimethylsiloxane are summarized in Table 1.

Table 1: Experimental conditions used for the encapsulation procedure.

Core material	Core/shell	Rotation speed (rpm)	Core + PMMA in CH_2Cl_2 (% wt.)	PVA (%wt.)	NaCl (%wt.)
PDMS-(2-NH_2)	3	600	14	1	3
PDMS-(4-COOH) / dodecane = 2	2	600	13	1	3

2.3 Characterization of microcapsules

To evaluate the morphology of the microcapsules along with the shell thickness, optical micrograph and scanning electron microscopy (SEM) images were acquired. To estimate the core content and assess the thermal stability of the microcapsules, thermogravimetric analysis (TGA) was performed in a temperature range starting from room temperature up to 800 °C with a heating rate of 10 °C min, under nitrogen flux. FTIR analysis was performed using a Jasco FT/IR-615 Fourier-transform infrared spectrometer, in absorption mode. In the case of PMMA shells, the analysis was carried out using a film of PMMA prepared by solvent casting in chloroform. In the case of microcapsules, the spectra were obtained by preparing IR windows with a mixture of microcapsules and KBr powder by tablet method.

2.4 Film preparation for corrosion tests

2.4.1 Reference samples

The sample for the corrosion tests was prepared by the following procedure. Q-panels of bare steel (type S-36) were used as substrates. The steel Q-panels are made from A1008 standard low-carbon steel plates with C < 0.15%, Mg < 0.6%, and a phosphorus and sulphur percentage lower than 0.03% and 0.035%, respectively. Before the application of the film, the Q-panels were washed and sonicated in an ethanol bath, to remove the residual organic impurities on the surface that could reduce the film adhesion. Then, a 24.4 µm (one mil) thick film of a standard epoxy primer (Interprotect white A+B, Akzonobel) was deposited on the Q-panel as an inter-layer and cured at room temperature for 3h. Afterward, a 203.2 µm (eight mils) thick film of an epoxy topcoat (Huntsman), composed of Araldite BY 158 (78% wt.) and Aradur 21 (22% wt.), was deposited on the Q-panel and cured at room temperature for 24 h.

2.4.2 Coatings with microcapsules

As for the sample without the microcapsules, a 24.4 µm (one mil) thick film of high-performance epoxy primer (Interprotect white A+B, Akzonobel) was deposited on the Q-panel as an inter-layer and cured at room temperature for 3h. Then, both PDMS-(2-NH_2) and PDMS-(4-COOH) microcapsules were imbedded at 20 phr content in the epoxy resin (Huntsman), composed of Araldite BY 158 (78% wt.) and Aradur 21 (22% wt.), using a weight ratio of 2/1 between PDMS-(2-NH_2) and PDMS-(4-COOH). Afterward, a 203.2 µm (eight mils) thick film of the epoxy/microcapsules mixture was deposited on the Q-panel and cured at room temperature for 24 h.

2.5 Characterization of films

The electrochemical characterization was performed using an AUTOLAB 302N potentiostat/galvanostat/FRA (Metrohm AG, Switzerland). A three electrodes arrangement was employed: a platinum ring as a counter electrode, an Ag/AgCl (3 M KCl) electrode as the reference one, and the coated samples being connected as the working electrode. The frequency ranged from 100 kHz to 10 mHz with 6 points per decade and 20 mV (peak-to-peak) amplitude of the sinusoidal potential signal on open-circuit potential (OCP). The immersed area was 16.6 cm^2. Electrochemical impedance spectroscopy (EIS) data-sets have been collected over intact and scratched coatings. The artificial defects consist of a 15 mm long scratch performed using a sharp cutting blade, which determined, therefore, its width. Diverse electrolytes were employed for EIS measurements: intact coatings were exposed to quiescent 0.5 M NaCl during about 3400h (about 140 days) whilst the scratched coatings were exposed to quiescent 0.1 M NaCl during 1000 h (about 40 days). In particular, the less concentrated solution has been employed to monitor more accurately the evolution of the electrochemical response of the protection system during immersion. ZSimpWin software has been used to fit the experimental data sets. An elemental mapping using Energy Dispersive X-Ray Spectroscopy (EDXS) during SEM analyses was used to characterize the scratched coatings during the immersion in 0.1 M NaCl.

3. Results and discussions

3.1 Microcapsule preparation and characterization

The microcapsule with a PMMA-based shell and a core consisting of either amino- or carboxylic acid-terminated PDMS were prepared via a solvent evaporation/extraction method schematically represented in Figure 1e. Very briefly, the core (PDMS oligomers) and the shell (PMMA) material

were dissolved in a volatile solvent, which is immiscible with water (CH_2Cl_2). By adding the core/shell solution in an aqueous solution containing a suitable colloidal stabilizer under vigorous mechanical stirring, the formation of an emulsion with a dispersed phase of PDMS oligomers/PMMA solution in a continuous aqueous phase occurred. After an appropriate emulsification time, the emulsion was poured in a proper amount of the same aqueous solution containing the colloidal stabilizer. Then, the evaporation of the volatile solvent at room temperature led to the formation of PMMA-based microcapsule shells, containing PDMS oligomers. NaCl was added to the aqueous solution to increase the interfacial tension between the colloidal stabilizer solution and the core materials. PDMS oligomers in fact exhibited an amphiphilic behavior and partially were dissolved in water during the emulsification without adding NaCl, due to the amine and carboxylic acid terminal end groups. By adding NaCl, the ionic strength of the aqueous solution and the interfacial tension between the emulsifying solution and the core materials were increased, thus lowering the affinity of core materials with water and facilitating the microencapsulation process.

Optical and SEM images show that spherical particles with a diameter, ranging from 20 to 70 μm, were obtained for microcapsules loaded with amine-terminated PDMS (Figure 2a and b). A very similar morphology was obtained for the microspheres containing carboxylic acid-terminated PDMS (Figure 2c and d). However, the average diameter seemed to be slightly higher in the latter case, due to the higher viscosity of the core material. As shown in Figure S2, the shell thickness for PDMS-(2-NH_2) containing microcapsules was nearly 2 μm, while the microcapsules loaded with carboxylic acid-terminated PDMS showed a slightly thicker shell of 2-3.5 μm.

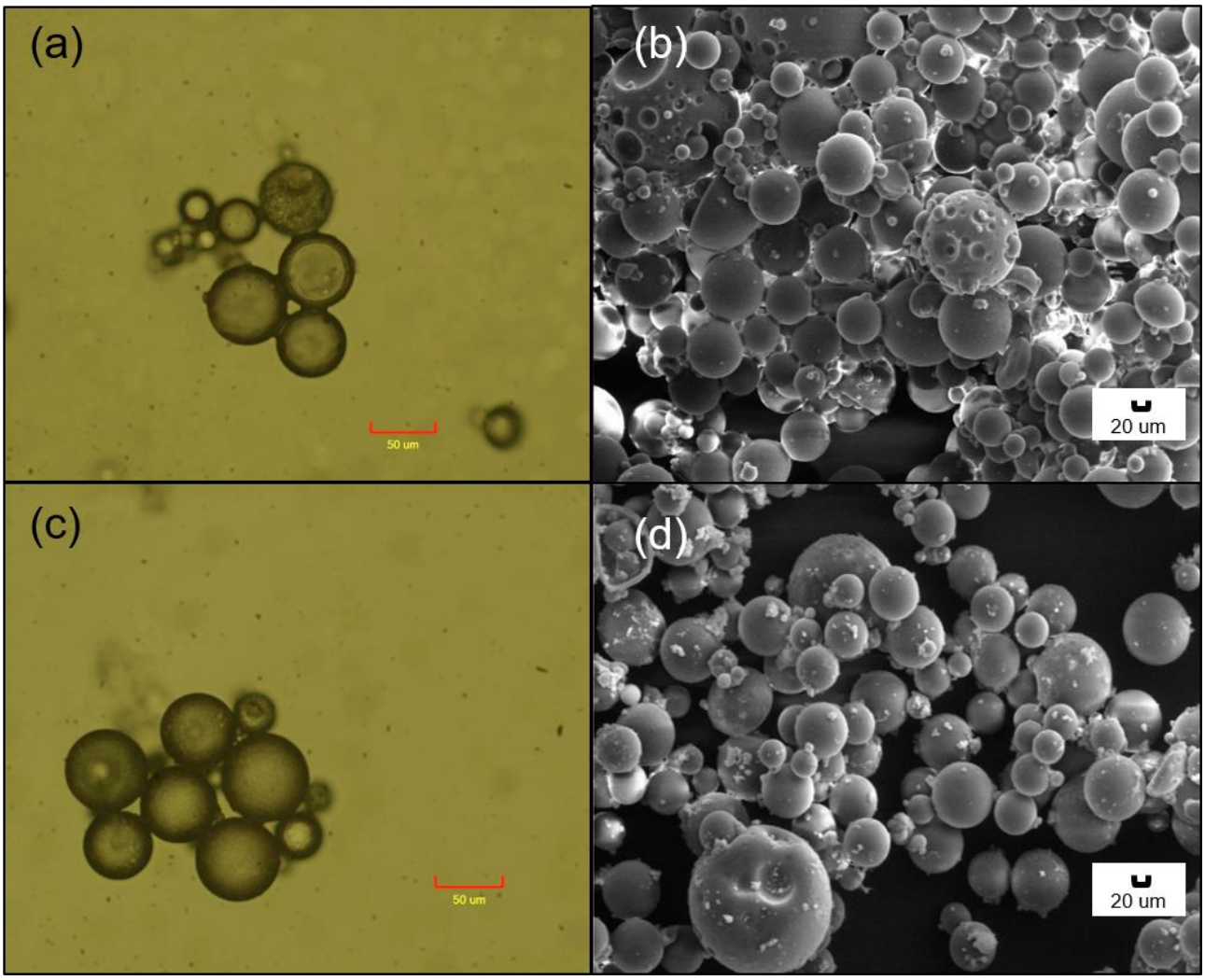

Figure 2. Optical microscope images (a and c) and SEM photographs (b and d) of the microspheres loaded (a and b) with amino-terminated PDMS oligomers and (c and d) with carboxylic acid-terminated PDMS oligomers.

TGA analysis was performed to investigate the thermal stability and the core content of the as-prepared microcapsules. As shown in Figure 3, no significant weight loss in the curves of microcapsules containing PDMS oligomers was observed up to a temperature of nearly 150 °C, indicating the possible use of these microcapsules also in coatings for high-temperature applications, when curing cycles with high temperature may be necessary. Figure 3a shows the comparison between the TGA curves of the PDMS-(2-NH_2) pure core, the PMMA pure shell, and the microcapsules loaded with PDMS-(2-NH_2). As shown in Figure 3a, the pure PMMA utilized for this work (Figure 3(a), black line) completely decomposed at nearly 405 °C, with a final residual weight of 1%. Considering the TGA curve of microcapsules loaded with amine-terminated PDMS, a much higher residual (~55%) was observed at 405 °C, with a further 20% mass decrease between 405 °C

and 450 °C, followed by a 35% decrease for temperatures up to 800 °C. Even though the pure core material (Figure 3a, green curve) showed a weight loss, which is approximately 20% at 405 °C, a portion of the core material was deposited on the external walls of the microcapsule shells and therefore the residual weight for the curve of microcapsules at the same temperature can be associated almost completely with the weight of the core material, loaded in the microcapsules. Consequently, a value of around 50% can be estimated for the core loading of PDMS-(2-NH_2) loaded microcapsules from these results.

A shown in Figure 3b, the pure PMMA shell of microcapsules loaded with PDMS-(4-COOH) (black line) decomposed nearly completely at 405°C, with a residual of 1%, as already observed for amine-terminated PDMS loaded microcapsule shell. Looking at the curve of microcapsules loaded with carboxyl acid terminated PDMS (orange line, Figure 3(b)), a small loss of weight in the temperature range between 150 °C and 200 °C can be observed. This finding can be associated with the loss of the dodecane, used as a solvent to decrease the viscosity of the core. Assuming also in this case that the residual weight of microcapsules at 405 °C could be associated almost completely with the core material, the estimation of the core loading is around 48%.

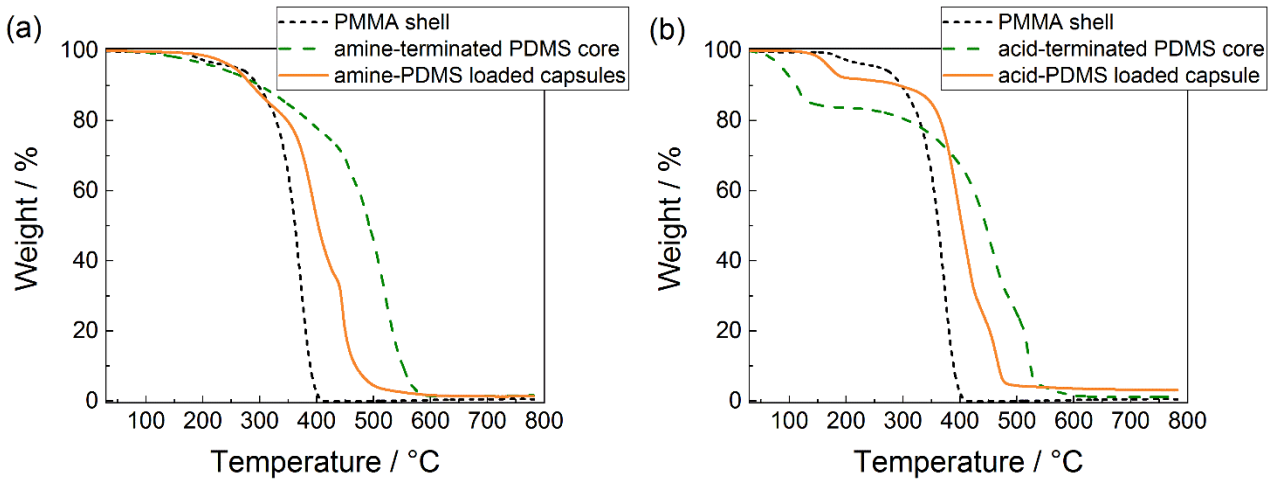

Figure 3. (a) TGA curves for microcapsules loaded with an amine-terminated PDMS oligomer, for the pure core (i.e. amine-terminated PDMS oligomer) and the pure PMMA shells; (b) TGA curves for microcapsules loaded with a carboxyl acid-terminated PDMS, for the pure core material (i.e. carboxylic acid-terminated PDMS oligomer) and the pure PMMA shell.

To characterize additionally the microcapsules obtained in this work, FTIR analysis of core materials, PMMA shells, and PMMA microcapsules, containing both PDMS-amine and PDMS-acid oligomers, was carried out and FTIR spectra are shown in Figure S1. PDMS characteristic peaks can be found

in the spectra of both the microcapsules spectra and both core materials. More specifically, the peaks between 789 and 796 cm^{-1} can be attributed to $-CH_3$ rocking and Si-C stretching in $Si-CH_3$, while the absorption between 1020–1074 cm^{-1} and 1259–1260 cm^{-1} can be respectively associated with Si-O-Si stretching and CH_3 deformation in $Si-CH_3$ [46]. In the spectrum of the pure carboxylic acid-terminated PDMS oligomers, a clear peak at 1720 cm^{-1} can be attributed to the stretching of carboxylic groups at the chain ends of the PDMS oligomers. For the same reason, this absorption peak is also present in the IR spectrum of PMMA microcapsules loaded with acid-terminated oligomers and it shows a higher broadness due to the presence of carbonyl groups of PMMA shells. Differently, the presence of primary amines in the pure amine-terminated oligomers is confirmed by a weak absorption band at 1560–1600 cm^{-1} attributed to the deformation vibrations of $-NH_2$ and also by some weak peaks in the region between 1430 and 1480 cm^{-1}, assignable to the deformation vibrations of $-CH_2$ groups bonded to primary amines [47]. Regarding the spectrum of the PMMA shells, the absorption band at 1720-1750 cm^{-1} can be attributed to the stretching of the carbonyl groups (C=O), which are present in PMMA chains [48]. The C=O stretching is also present with a lower intensity by the loaded microcapsule spectra. Moreover, the peak at around 2952 cm^{-1} can be associated with the stretching of CH bonds in methyl and methylene groups, which are present in PMMA shells and also in PDMS oligomers.

3.2 Characterization of microcapsule-loaded coatings

The evolution with immersion time in 0.5M NaCl of the impedance spectra collected over the intact coatings is reported in Figure 4. According to the cross-sectional images of the coatings, the microcapsules were embedded in the epoxy matrix and seemed not to be in contact with each other. The dispersion appeared not perfectly homogenous, but a clustering effect was not observed. As shown in Figure 4, the dried films were found to have a thickness of 120-130 µm.

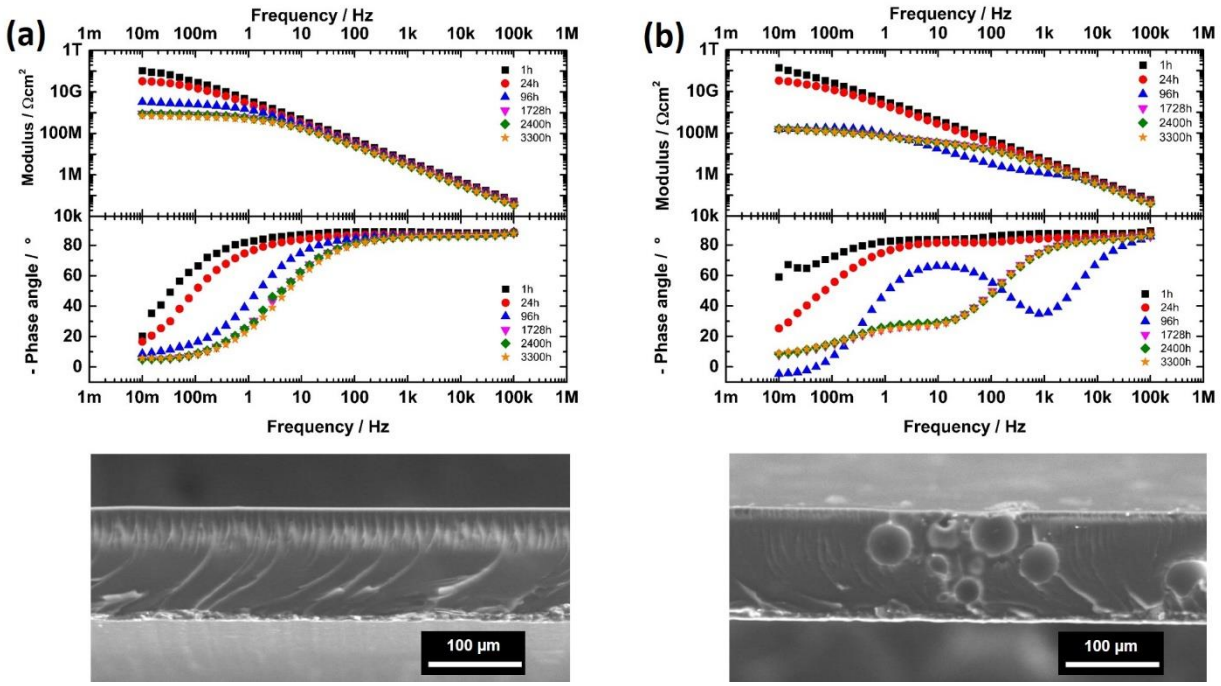

Figure 4. Impedance (modulus and phase) diagrams during the immersion in 0.5M NaCl and cross-section SEM micrographs: (a) the reference coating and (b) the microcapsule-loaded coating.

At the beginning of the immersion, both coatings showed a capacitive response in the middle-high-frequency range and a resistive response in the low-frequency domain. During the very first hours of immersion, the impedance modulus in the low-frequency range (at 0.01 Hz, $|Z|_{0.01}$) was about 10^{11} Ωcm^2 for both the microcapsule-loaded coatings and the reference coatings. With time elapsed, a more marked decrease of the $|Z|_{0.01}$ was observed for the coatings containing capsules, compared to the reference. After about 100 h of immersion, a relaxation process in the middle-low frequency range appeared in the EIS spectrum of the coatings containing capsules, suggesting the onset of a corrosion process at the metal-polymer interface. A similar phenomenon was not observed in the investigated frequency range for the control sample thoroughly the entire immersion time. The evolution of the impedance and phase angle spectra suggests that the presence of the microcapsules can be detrimental to a certain extent for barrier properties of the coating. Thus, the permeation of the electrolyte promoted the onset of an under-paint corrosion process. To get some insight into the evolution of the barrier properties of the investigated materials, the EIS raw data sets were analyzed using a non-linear least squares regression procedure. For this purpose, the equivalent electrical circuits (e.e.c.) depicted in Figure 5 were employed. Notice that constant phase elements (CPEs) were used instead of pure capacitances to account for the surface inhomogeneity, roughness, and the current and potential distribution due to the electrode geometry [49, 50]. The impedance representation of a CPE is $Z_{CPE}=1/[Q(j\omega)^{\alpha}]$, where Q is the CPE parameter, ω is the angular frequency, j is the imaginary unit

(j=√-1) and the exponent α is the frequency dispersion factor (being -1< α<1) [51]. The numerical values of the parameters Q and α obtained from the fitting are discussed in this manuscript.

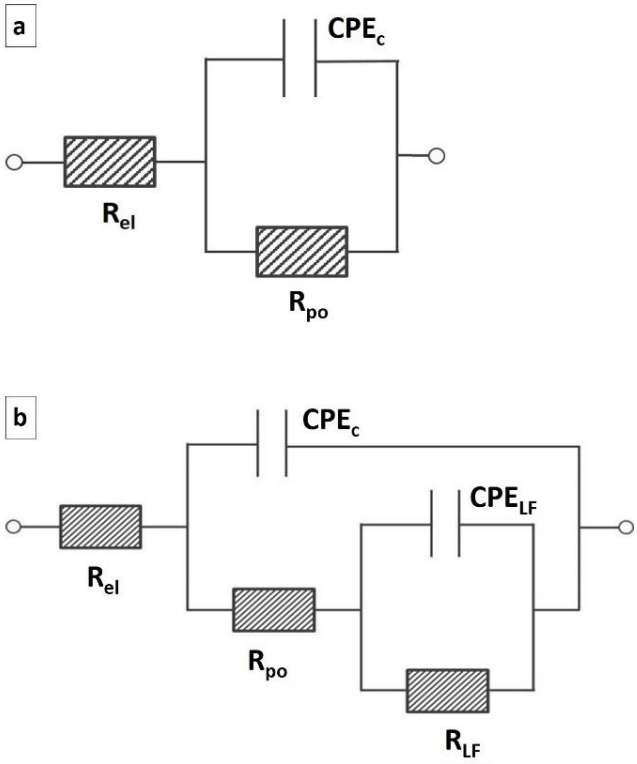

Figure 5. Equivalent electrical networks employed to fit the experimental EIS raw data sets: (a) for the intact coating and (b) for the coating containing microcapsules.

In the circuit depicted in Figure 5a, R_{el} indicates the electrolyte's resistance, CPE_c the constant phase element (CPE) associated with the dielectric properties of the coating and R_{po} its pore resistance [52]. Once the relaxation process in the middle-low frequency range appeared in the phase angle plot of the coating containing capsules, the circuit showed in Figure 5b was employed to include the additional time constant. Accordingly, R_{el}, CPE_c, and R_{po} maintain the previously described meaning while the parameters CPE_{LF} and R_{LF} account for the faradic process occurring at the metal/electrolyte interface. The evolution with the immersion time of the pore resistance for the investigated coatings is reported in Figure 6 together with the measured potential.

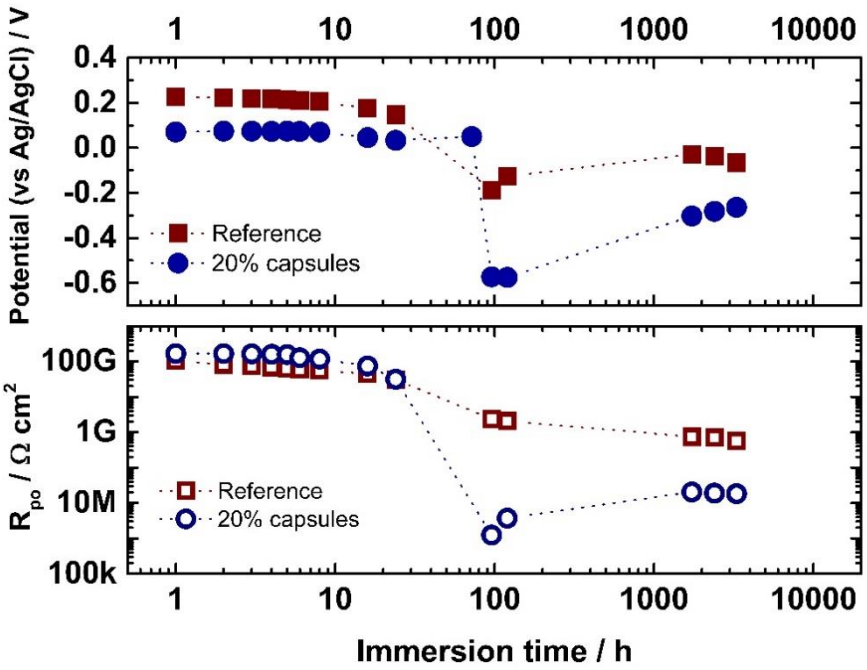

Figure 6. Time-variations of R_{po} and potential for investigated intact samples during immersion in 0.1 M NaCl.

Notice that the potential decreased from 0.1 V to -0.6 V for the samples containing capsules between 50-100 h of continuous immersion in the electrolyte. In correspondence with the steep drop of the potential observed for the coatings containing capsules, the R_{po} values are reduced by about four orders of magnitude, thus suggesting a significant permeation of the electrolyte through the coatings. A less marked decrease in potential (from 0.2 V to -0.1V) and R_{po} (about one-two orders of magnitude) was also observed for the reference samples. These findings further suggest that, to a certain extent, the presence of the microcapsules is detrimental to the barrier properties of the paint layer. Our interpretation is that the presence of microcapsules promoted the formation of preferential pathways at the capsule/matrix interface that allowed penetration of the electrolyte through the coating, even in the absence of artificial defects such as crosscuts. Similar behavior was also observed by other authors [53]. The increase in the corrosion potential for prolonged immersion time is attributed to the development of cathodic areas [54] and to the resulting contributions from charge transfer and mass transport reactions occurring in pores filled with corrosion products [55]. All the circuit parameters, obtained by regression using the e.e.c. described in Figure 5, are summarized in Table 1.

Table 2. Electrical parameters obtained by regression of the circuits depicted in Figure 5

Reference						
Time h	**R_{po}** GΩ cm^2	**Q_c** pΩ^{-1}s$^{\alpha}$cm^{-2}	**α_c**	**R_{LF}** GΩ cm^2	**Q_{LF}** nΩ^{-1}s$^{\alpha}$cm^{-2}	**α_{LF}**
1	103.9	42.3	0.97	-	-	-
8	56.2	54.6	0.96	-	-	-
16	44.3	57.4	0.95	-	-	-
24	30.8	63.1	0.95	-	-	-
96	2.4	74.3	0.94	-	-	-
120	2.1	78.5	0.94	-	-	-
1728	0.7	104.1	0.93	-	-	-
2400	0.7	106.9	0.93	-	-	-
3300	0.6	110.0	0.93	-	-	-
20% microcapsules loaded						
Time h	**R_{po}** GΩ cm^2	**Q_c** pΩ^{-1}s$^{\alpha}$cm^{-2}	**α_c**	**R_{LF}** GΩ cm^2	**Q_{LF}** nΩ^{-1}s$^{\alpha}$cm^{-2}	**α_{LF}**
1	167.9	56.6	0.94	-	-	-
8	117.3	73.0	0.92	-	-	-
16	74.7	78.6	0.92	-	-	-
24	31.4	89.3	0.91	-	-	-
96	0.001	70.4	0.95	0.19	1.7	0.82
120	0.004	106.8	0.91	0.14	4.8	0.88
1728	0.020	94.5	0.93	0.16	5.2	0.50
2400	0.019	99.2	0.93	0.16	5.3	0.51
3300	0.018	101.1	0.93	0.15	6.1	0.48

The exponent α_c values of the CPEs range between 0.97-0.93 and 0.94-0.91 for the reference and microcapsule-loaded coatings, respectively. Thus, the numerical values of the parameter Q_c do not correspond to a pure capacitance, even if it is likely to reflect the dielectric properties of the coatings. The EIS response of the scratched coatings during 1000 h of immersion in 0.1M NaCl is reported in Figure 7. In the beginning, the response of the sample was dominated by the small impedance of the scribe, and the $|Z|_{0.01}$ is approximately $10^4 – 10^5$ Ωcm^2. It should be mentioned that the scratches were hand-made by using a cutter and, thus, minor differences in the initial EIS spectra were due to slight variations in the dimension of the artificial scribe. Having said this, as far as Figure 7 is concerned, the difference was limited to the measurement collected after the first hours of immersion and, from the 8th hour of immersion, the impedance in the low-frequency range was comparable at about 100 kΩcm^2. Moreover, the spectra collected after the very first hours were quite scattered from one sample to another but they aligned within the first day of immersion.

With time elapsed, $|Z|_{0.01}$ increased to about 10^7 Ωcm^2 for the microcapsule-loaded coating and about 10^6 Ωcm^2 for the reference sample. Considering the evolution of the phase angle spectra in Figure 7b, after the very first hours of immersion, a relaxation process in the high-frequency domain gradually appeared. In the microcapsule-loaded coating case, this was accompanied by a marked rise in impedance modulus (Figure 7a). The shape of the impedance modulus in the high-frequency domain seemed to resemble a capacitive behavior that was more and more marked over time. This phenomenon was attributed to the effect of the ruptured microcapsules, which released the reactive

species in the scribe, thus promoting the healing of the epoxy coating. According to the impedance modulus and phase plots in Figure 7b, two-time constants were observed. The relaxation process located in the high-frequency domain was attributed to the gradual healing of the artificial scribe, thanks to the release of chemical species from the microcapsules. The second time constant in the low-frequency domain was attributed to the faradic process occurring in the scribe and under-paint at the metal/solution interface.

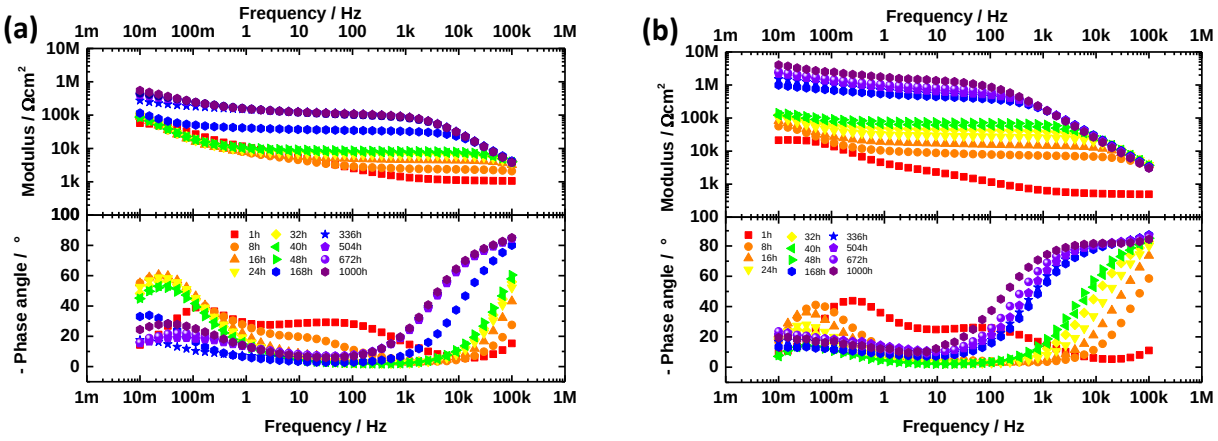

Figure 7. Impedance modulus and phase time evolution collected for the scratched coatings during immersion in 0.1M NaCl: (a) reference coating and (b) microcapsule-loaded coating.

The regression of the obtained impedance spectra in the whole investigated frequency domain was attempted employing the e.e.c. suggested in the literature for disbonded coatings [55] or coated metals undergoing loss of adhesion [56]. Alternatively, the models that introduce restricted finite-length diffusion elements to account for the blocking effect to oxygen transport provided by corrosion products in the scribe were considered [57].

The e.e.c. revealed to be suitable to fit the relaxation process in the high-frequency domain (attributed to the scratched coating) but failed to model the low-frequency relaxation process (attributed to the faradic process occurring at different sites located at the metal/coating interface). This issue was attributed to the intrinsic limitations of extracting high impedance data from the sites at the metal/coating interface when the obtained impedance data is dominated by the small impedance value of the scratch [58]. In our case, it was not possible to determine the parameters associated with the interface phenomena by regression of any of the circuits proposed in the literature [55, 56].

For this reason, the regression of the experimental EIS data sets was limited to the investigation of the middle-high frequency domain to determine the evolution of the physical parameters associated with the scratched coatings. In particular, the equivalent electrical network depicted in Figure 5a was

employed. However, in this case, the physical meaning of the equivalent electrical parameters is different: in the parallel RQ circuit of Figure 5a, the resistance is associated with the resistive contribution of the scratched coating (R_{sc}) and the CPE to its dielectric behavior (described by parameters Q_c and α_c). The chi-squared values corresponding to the regression of the experimental EIS data sets in the middle-high frequency range were found to be 10^{-4} or lower.

Figure 8 shows the time-variations of R_{sc} and corrosion potential of investigated scratched coatings during immersion in 0.1 M NaCl (the electrical parameters obtained by the regression are summarized in Table 3).

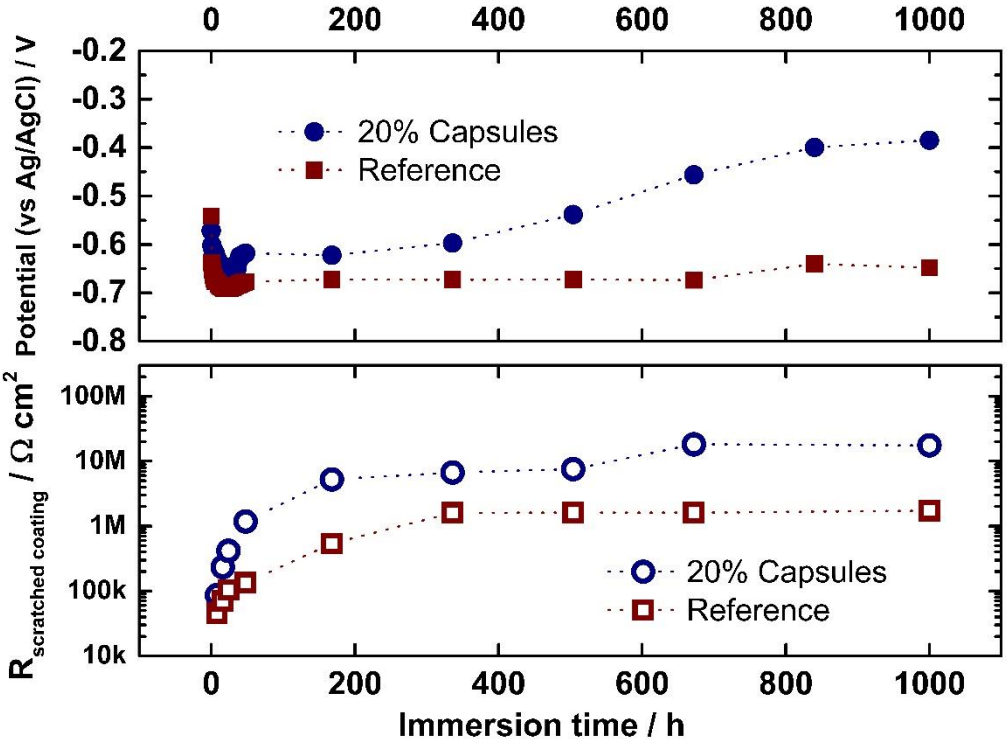

Figure 8. Time-variations of R_{sc} and potential for investigated scratches during the immersion in 0.1M NaCl.

Table 3. Electrical parameters obtained by regression of the circuit depicted in Figure 5a.

	Reference			20% microcapsules loaded		
Time (h)	R_{sc} MΩcm²	Q_c pΩ⁻¹s^αcm⁻²	α_c	R_{sc} MΩcm²	Q_c pΩ⁻¹s^αcm⁻²	α_c
8	0.046	22.0	0.99	0.086	62.7	0.93
16	0.070	20.5	1.00	0.234	48.0	0.96
24	0.104	28.0	0.98	0.416	56.4	0.94
48	0.134	31.0	0.97	1.181	80.2	0.92
192	0.539	58.1	0.93	5.239	80.8	0.92
360	1.606	70.6	0.92	6.702	80.2	0.93
504	1.608	79.1	0.92	7.543	80.6	0.93
840	1.609	80.2	0.92	18.197	97.9	0.92
1000	1.732	78.3	0.92	17.516	101.1	0.92

At the beginning of the immersion, the corrosion potential measured over the scratched coatings (-0.6 - -0.7 V) reflected that of mild steel [59] since there was direct contact between the electrolyte and the mild steel substrate. Accordingly, R_{sc} was below 10^5 Ωcm^2 since the electrochemical response was dominated by the small impedance value of the artificial defects. With time elapsed, it was possible to observe that the R_{sc} gradually increased for both the microcapsule-loaded and reference scratched coatings. In particular, the microcapsule-loaded coating showed an R_{sc} value, which grew to about 17.5 10^6 Ωcm^2 during immersion time along with an increase in the corrosion potential value to -0.4 V.

On the other hand, the reference coating showed a more limited increase in R_{sc} (to about 1.73 10^6 Ωcm^2) during immersion time, and an almost stable value of the corrosion potential around -0.65 V. These findings suggest that the presence of the microcapsules in the coating induced a gradual increase in the protection properties during immersion time. The visual inspection of the scratch area on the coating containing capsules further confirms the authors' hypothesis: during immersion time in 0.1M NaCl, a partial sealing of the scratch can be observed from 100 to 1000 h of immersion (Figure 9). As far as the naked-eyed inspection is concerned, the scratch seems almost completely sealed at the end of the immersion time.

Figure 9. Visual appearance of the scribes during 1000 h of continuous immersion in 0.1M NaCl.

Accordingly, the observed improvement in barrier properties of the coatings along with the observed partial sealing of the scratch can likely be attributed to the amino- and carboxylic acid- terminated PDMS oligomers released in the scribe to form a supramolecular polymer network. When the microcapsules are ruptured, the functional constituents are released, transported to the defected area, and react to repair the damage in the coating. It should be noted that the improvement in R_{sc} for the microcapsule-loaded coating was significantly more pronounced compared to the control sample regardless of the lower barrier properties of the coating itself, as demonstrated by EIS collected over intact samples. As far as the CPE parameters are concerned (see Table 3), notice that the Q_c values resemble those measured on intact coatings. This fact further supports the authors' hypothesis related

to the attribution of the high-frequency relaxation process observed in the EIS spectra to the electrochemical response of the scratched coatings. Also, in this case, several times the value of α_c is much lower than 1 and therefore it is not possible to attribute a clear physical meaning to Q_c. When the value of α_c summarized in Table 3 is equal to unity, the corresponding Q_c values can be considered the capacitance of a scratched coating.

Based on these findings, the healing of the epoxy coating is reflected in the rise in R_{sc}, in the ennoblement of corrosion potential and is further confirmed by the visual inspection of the scribe after the 1000 h of continuous immersion in 0.1 M NaCl (Figure 10).

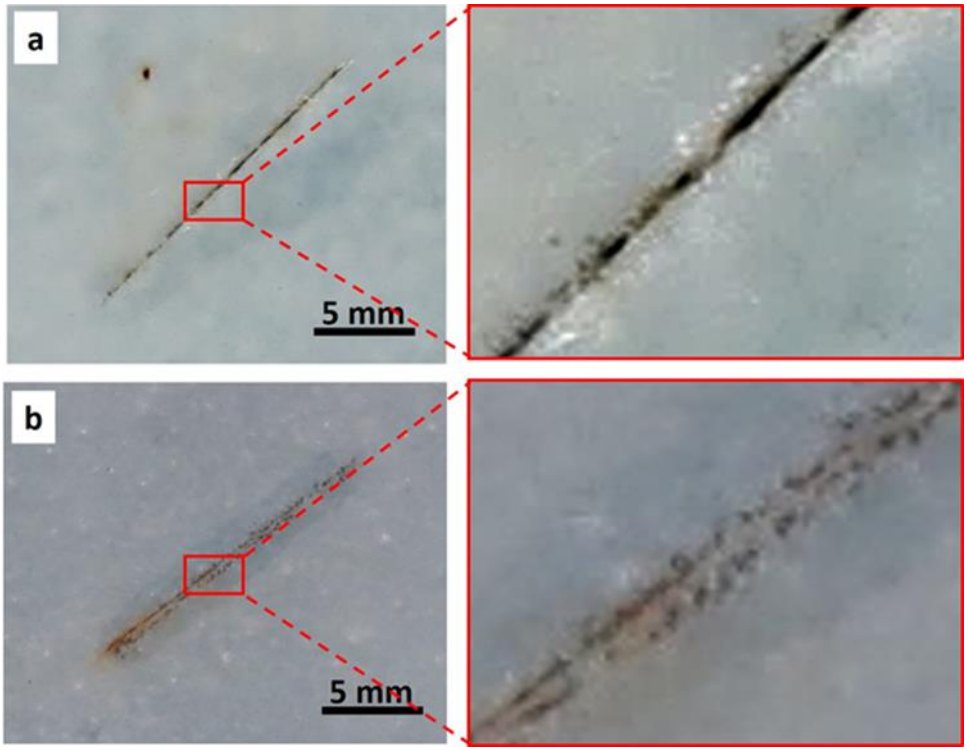

Figure 10. Visual appearance of the scribes after 1000 h of continuous immersion in 0.1M NaCl: (a) reference coating and (b) microcapsule-loaded coating.

From Figure 10b, it seems that the scratch was at least partially sealed by the supramolecular polymer network developed in-situ upon reactants release from the microcapsules. This was not observed for the reference coating shown in Figure 10a and, in this case, the scribe was still completely open.

It should be noted that the reference sample also showed a certain increase in R_{sc}, although limited and not accompanied by a variation of the corrosion potential. In this case, since no healing species were embedded in the coatings, the apparent improvement of the barrier properties observed for the reference coating was likely to be due to the formation of insoluble corrosion products in the scratched area. According to a previous literature report [60], insoluble corrosion products can plug the

scratched area, thus leading to an increase in transfer resistances, which can become limited by diffusion through the scratch filled with corrosion products. This phenomenon was actually much more pronounced for the coatings containing microcapsules, where the release of healing species was believed to take place together with the development of insoluble corrosion products. Moreover, after 1000 h of immersion in 0.1 M NaCl, it is possible to observe the presence of a whitish material in the scribe performed on the microcapsule containing coating, while exclusively iron corrosion products can be observed in the scribe performed on the standard coating (Figure 10a). Therefore, for prolonged immersion, the sealing effect was enhanced and effective for the coating containing microcapsules, due to the release of healing species.

An elemental mapping using Energy Dispersive X-Ray Spectroscopy (EDXS) during SEM analyses was used to evaluate further the healing ability of the coatings containing microcapsules. EDXS maps were acquired on different portions of the scratches after 200 h of immersion in 0.1 M NaCl. As shown in Figure S3, a more intense Si signal was detected in some points of the intact coating (in correspondence with the microcapsules) and in other regions over the scratched zone, which appeared partially repaired by a silicon-based material, bridging the edges of the scratch. This finding confirms the presence of a repairing process, even at only 200 h of immersion in 0.1 M NaCl, due to the formation of the supramolecular network between PDMS-(2-NH_2) and PDMS-(4-COOH) oligomers poured into the scratch.

4. Conclusions

A self-healing system based on supramolecular acid-base interactions with potential applications in anticorrosive coatings was developed.

Microcapsules containing amino- and carboxylic acid-terminated polydimethylsiloxane (PDMS) oligomers were successfully synthesized via the solvent evaporation method. To facilitate the encapsulation process, NaCl was needed to increase the interfacial tension between the colloidal stabilizer solution and the core materials, leading to an increase in the core loading. SEM and optical images showed the formation of spherical particles with a diameter, ranging from 20 to 70 µm. The microcapsules containing carboxylic acid-terminated PDMS exhibited a slightly higher diameter than the amino-terminated PDMS microcapsules. A core loading of around 50% was estimated for carboxylic acid-terminated PDMS-loaded microcapsules and of 48% for amino-terminated PDMS through TGA analyses.

EIS results collected over epoxy coatings, modified with microcapsules loaded with functional PDMS oligomers and deposited on mild steel substrates revealed that the presence of the microcapsules

promoted a slight decrease in the barrier properties of the paint layer. However, it should be noted that the pore resistance remained higher than 10 MΩcm² even for prolonged immersion (3000 h) in 0.1 M NaCl. Moreover, EIS results of scratched coatings, modified with microcapsules loaded with functional PDMS oligomers and deposited on mild steel substrates, showed an impedance modulus in the low and medium-high frequency domains higher than the reference coating in long-term immersions in NaCl solutions. Moreover, the presence of microcapsules induced a two order of magnitude increase in the scratched coating resistance during the long-term immersions, accompanied by an increase of corrosion potential, and conferred a more pronounced capacitive behavior to coated steel. These electrochemical results revealed that the epoxy-coated steel with PDMS microcapsules gained an enhanced corrosion protective ability in case of scratch damage, due to the formation of supramolecular ionic interactions between the amino- and carboxylic acid-terminated PDMS. A self-healing process, induced by the release of functional ionic PDMS embedded in microcapsules, was confirmed by a visual inspection of scratch damaged coatings after 1000 h of immersion in NaCl solution. This study, therefore, demonstrates that the addition of encapsulated functional PDMS oligomer to coatings is an effective system for the corrosion protection of steel surfaces.

Acknowledgments

The authors would like to thank Solvay Specialty Polymer S.p.A for providing polymer samples and for stimulating discussions.

References

[1] C.M. Hansson, The Impact of Corrosion on Society, Metall. Mater. Trans. A 42 (2011) 2952-2962. https://doi.org/10.1007/s11661-011-0703-2
[2] N.H. Othman, M. Che Ismail, M. Mustapha, N. Sallih, K.E. Kee, R. Ahmad Jaal, Graphene-based polymer nanocomposites as barrier coatings for corrosion protection, Prog. Org. Coat. 135 (2019) 82-99. https://doi.org/10.1016/j.porgcoat.2019.05.030
[3] G. Koch, 1 - Cost of corrosion, in: A.M. El-Sherik (Ed.) Trends in Oil and Gas Corrosion Research and Technologies, Woodhead Publishing, Boston, 2017, pp. 3-30.
[4] O.S.I. Fayomi, I.G. Akande, S. Odigie, Economic Impact of Corrosion in Oil Sectors and Prevention: An Overview, J. Phys.: Conf. Ser. 1378 (2019) 022037. https://doi.org/10.1088/1742-6596/1378/2/022037
[5] R.B. Figueira, Hybrid Sol–gel Coatings for Corrosion Mitigation: A Critical Review, Polymers 12 (2020) 689. https://doi.org/10.3390/polym12030689
[6] C. Verma, L.O. Olasunkanmi, E.D. Akpan, M.A. Quraishi, O. Dagdag, M. El Gouri, E.-S.M. Sherif, E.E. Ebenso, Epoxy resins as anticorrosive polymeric materials: A review, React. Funct. Polym. 156 (2020) 104741. https://doi.org/10.1016/j.reactfunctpolym.2020.104741
[7] U. Riaz, C. Nwaoha, S.M. Ashraf, Recent advances in corrosion protective composite coatings based on conducting polymers and natural resource derived polymers, Prog. Org. Coat. 77 (2014) 743-756. https://doi.org/10.1016/j.porgcoat.2014.01.004
[8] A.W. Momber, M. Irmer, T. Marquardt, Effects of polymer hardness on the abrasive wear resistance of thick organic offshore coatings, Prog. Org. Coat. 146 (2020) 105720. https://doi.org/10.1016/j.porgcoat.2020.105720
[9] T.A. Truc, T.T. Thuy, V.K. Oanh, T.T.X. Hang, A.S. Nguyen, N. Caussé, N. Pébère, 8-hydroxyquinoline-modified clay incorporated in an epoxy coating for the corrosion protection of carbon steel, Surfaces and Interfaces 14 (2019) 26-33. https://doi.org/10.1016/j.surfin.2018.10.007
[10] M. Zheludkevich, Self-Healing Anticorrosion Coatings, in: Self-Healing Materials, 2008, pp. 101-139.
[11] S.J. García, H.R. Fischer, S. van der Zwaag, A critical appraisal of the potential of self healing polymeric coatings, Prog. Org. Coat. 72 (2011) 211-221. https://doi.org/10.1016/j.porgcoat.2011.06.016
[12] M.D. Hager, P. Greil, C. Leyens, S. van der Zwaag, U.S. Schubert, Self-healing materials, Adv. Mater. 22 (2010) 5424-5430. https://doi.org/10.1002/adma.201003036
[13] D. Döhler, P. Michael, W. Binder, Principles of Self-Healing Polymers, in: W.H. Binder (Ed.) Self-Healing Polymers, Wiley-VCH Verlag GmbH & Co., 2013, pp. 5-60.
[14] G. Cui, Z. Bi, S. Wang, J. Liu, X. Xing, Z. Li, B. Wang, A comprehensive review on smart anti-corrosive coatings, Prog. Org. Coat. 148 (2020) 105821. https://doi.org/10.1016/j.porgcoat.2020.105821
[15] S. Habib, R.A. Shakoor, R. Kahraman, A focused review on smart carriers tailored for corrosion protection: Developments, applications, and challenges, Prog. Org. Coat. 154 (2021) 106218. https://doi.org/10.1016/j.porgcoat.2021.106218
[16] M. Attaei, L.M. Calado, Y. Morozov, M.G. Taryba, R.A. Shakoor, R. Kahraman, A.C. Marques, M.F. Montemor, Smart epoxy coating modified with isophorone diisocyanate microcapsules and cerium organophosphate for multilevel corrosion protection of carbon steel, Prog. Org. Coat. 147 (2020) 105864. https://doi.org/10.1016/j.porgcoat.2020.105864
[17] L. Gonzalez, M. Kostrzewska, B.G. Ma, L. Li, J.H. Hansen, S. Hvilsted, A.L. Skov, Preparation and Characterization of Silicone Liquid Core/Polymer Shell Microcapsules via Internal Phase Separation, Macromol. Mater. Eng. 299 (2014) 1259-1267. https://doi.org/10.1002/mame.201400020

[18] D. Crespy, Y. Zhao, Preparation of Nanocapsules and Core–Shell Nanofibers for Extrinsic Self-Healing Materials, in: W.H. Binder (Ed.) Self-Healing Polymers, Wiley-VCH Verlag GmbH & Co., 2013, pp. 247-271.
[19] G.O. Fanger, What Good Are Microcapsules, Chemtech 4 (1974) 397-405.
[20] G.L. Gardner, Manufacturing encapsulated products, Chem. Eng. Prog. 62 (1966) 87–91.
[21] D.Y. Zhu, M.Z. Rong, M.Q. Zhang, Self-healing polymeric materials based on microencapsulated healing agents: From design to preparation, Prog. Polym. Sci. 49-50 (2015) 175-220. https://doi.org/10.1016/j.progpolymsci.2015.07.002
[22] S. Leclercq, K.R. Harlander, G.A. Reineccius, Formation and characterization of microcapsules by complex coacervation with liquid or solid aroma cores, Flavour Frag J 24 (2009) 17-24. https://doi.org/10.1002/ffj.1911
[23] E. Piacentini, L. Giorno, M.M. Dragosavac, G.T. Vladisavljević, R.G. Holdich, Microencapsulation of oil droplets using cold water fish gelatine/gum arabic complex coacervation by membrane emulsification, Food Research International 53 (2013) 362-372. https://doi.org/10.1016/j.foodres.2013.04.012
[24] E.N. Brown, M.R. Kessler, N.R. Sottos, S.R. White, In situ poly(urea-formaldehyde) microencapsulation of dicyclopentadiene, J. Microencapsul. 20 (2003) 719-730. https://doi.org/10.1080/0265204031000154160
[25] D.M. Schlemper, S.H. Pezzin, Self-healing epoxy coatings containing microcapsules filled with different amine compounds – A comparison study, Prog. Org. Coat. 156 (2021) 106258. https://doi.org/10.1016/j.porgcoat.2021.106258
[26] A.B.W. Brochu, W.J. Chyan, W.M. Reichert, Microencapsulation of 2-octylcyanoacrylate tissue adhesive for self-healing acrylic bone cement, J. Biomed. Mater. Res. B 100B (2012) 1764-1772. https://doi.org/10.1002/jbm.b.32743
[27] O.D. Velev, K. Furusawa, K. Nagayama, Assembly of latex particles by using emulsion droplets as templates .2. Ball-like and composite aggregates, Langmuir 12 (1996) 2385-2391. https://doi.org/10.1021/La950679y
[28] O.D. Velev, K. Furusawa, K. Nagayama, Assembly of latex particles by using emulsion droplets as templates .1. Microstructured hollow spheres, Langmuir 12 (1996) 2374-2384. https://doi.org/10.1021/La9506786
[29] O.D. Velev, K. Nagayama, Assembly of latex particles by using emulsion droplets .3. Reverse (water in oil) system, Langmuir 13 (1997) 1856-1859. https://doi.org/10.1021/La960652u
[30] W.H. Binder, Self-Healing Polymers: From Principles to Applications, Wiley-VCH Verlag GmbH & Co., 2013.
[31] A. Loxley, B. Vincent, Preparation of poly(methylmethacrylate) microcapsules with liquid cores, J Colloid Interf Sci 208 (1998) 49-62. https://doi.org/10.1006/jcis.1998.5698
[32] F. Ahangaran, M. Hayaty, A.H. Navarchian, Morphological study of polymethyl methacrylate microcapsules filled with self-healing agents, Appl. Surf. Sci. 399 (2017) 721-731. https://doi.org/10.1016/j.apsusc.2016.12.116
[33] M. Naveed, M. Rabnawaz, A. Khan, M.O. Tuhin, Dual-Layer Approach toward Self-Healing and Self-Cleaning Polyurethane Thermosets, Polymers 11 (2019) 1849.
[34] J. Wang, C. Lv, Z. Li, J. Zheng, Facile Preparation of Polydimethylsiloxane Elastomer with Self-Healing Property and Remoldability Based on Diels–Alder Chemistry, Macromol. Mater. Eng. 303 (2018) 1800089. https://doi.org/10.1002/mame.201800089
[35] G. Chen, Z. Sun, Y. Wang, J. Zheng, S. Wen, J. Zhang, L. Wang, J. Hou, C. Lin, Z. Yue, Designed preparation of silicone protective materials with controlled self-healing and toughness properties, Prog. Org. Coat. 140 (2020) 105483. https://doi.org/10.1016/j.porgcoat.2019.105483
[36] U. Eduok, Z. Xu, J. Szpunar, Fabricating protective silica/PMDS composite films for Mg alloy: Correlating bulk silica reinforcement with barrier performance, Journal of Non-Crystalline Solids 485 (2018) 47-56. https://doi.org/10.1016/j.jnoncrysol.2018.01.037

[37] X. Sun, R. Chen, X. Gao, Q. Liu, J. Liu, H. Zhang, J. Yu, P. Liu, K. Takahashi, J. Wang, Fabrication of epoxy modified polysiloxane with enhanced mechanical properties for marine antifouling application, European Polymer Journal 117 (2019) 77-85. https://doi.org/10.1016/j.eurpolymj.2019.05.002
[38] R. Suriano, O. Boumezgane, C. Tonelli, S. Turri, Viscoelastic properties and self-healing behavior in a family of supramolecular ionic blends from silicone functional oligomers, Polymers for Advanced Technologies 31 (2020) 3247-3257. https://doi.org/10.1002/pat.5049
[39] B. Di Credico, M. Levi, S. Turri, An efficient method for the output of new self-repairing materials through a reactive isocyanate encapsulation, European Polymer Journal 49 (2013) 2467-2476. https://doi.org/10.1016/j.eurpolymj.2013.02.006
[40] M. Behzadnasab, S.M. Mirabedini, M. Esfandeh, R.R. Farnood, Evaluation of corrosion performance of a self-healing epoxy-based coating containing linseed oil-filled microcapsules via electrochemical impedance spectroscopy, Prog. Org. Coat. 105 (2017) 212-224. https://doi.org/10.1016/j.porgcoat.2017.01.006
[41] K. Chakraborty, F. De Campo, A. Gopal, G. Padmanaban, C. Tonelli, V. Valodkar, Compositions of ionisable organosiloxane polymers, patent WO/2020/030678A1, 2020.
[42] C. Hamon, R.D.C. Pieri, Floryan;, C.A.P. Tonelli, A multilayer assembly for electrochemical cells, patent WO/2019/101698, 2019.
[43] S. Meeker, F. De Campo, C.A.P. Tonelli, G. Marchionni, A method for preventing corrosion of metal articles, patent WO/2019/101697, 2019.
[44] C.A.P. Tonelli, G. Marchionni, S. Barbieri, E. Denisov, G. Carignano, Method for preventing corrosion of metal articles, patent WO/2018/078001, 2018.
[45] Q. Li, A.K. Mishra, N.H. Kim, T. Kuila, K.T. Lau, J.H. Lee, Effects of processing conditions of poly(methylmethacrylate) encapsulated liquid curing agent on the properties of self-healing composites, Compos Part B-Eng 49 (2013) 6-15. https://doi.org/10.1016/j.compositesb.2013.01.011
[46] L.M. Johnson, L. Gao, C.W. Shields Iv, M. Smith, K. Efimenko, K. Cushing, J. Genzer, G.P. López, Elastomeric microparticles for acoustic mediated bioseparations, Journal of Nanobiotechnology 11 (2013) 22. 10.1186/1477-3155-11-22
[47] G. Socrates, Infrared and Raman Characteristic Group Frequencies: Tables and Charts, John Wiley & Sons Ltd, Chichester, 2004.
[48] F.J. Tommasini, L. da Cunha Ferreira, G.P.T. Lucas, V. de Oliveira Aguiar, M.H. Prado da Silva, L.F. da Mota Rocha, M.d.F. Vieira Marques, Poly(Methyl Methacrylate)-SiC Nanocomposites Prepared Through in Situ Polymerization, Materials Research 21 (2018) e20180086. 10.1590/1980-5373-MR-2018-0086
[49] G.J. Brug, A.L.G. van den Eeden, M. Sluyters-Rehbach, J.H. Sluyters, The analysis of electrode impedances complicated by the presence of a constant phase element, Journal of Electroanalytical Chemistry and Interfacial Electrochemistry 176 (1984) 275-295. https://doi.org/10.1016/S0022-0728(84)80324-1
[50] J.-B. Jorcin, M.E. Orazem, N. Pébère, B. Tribollet, CPE analysis by local electrochemical impedance spectroscopy, Electrochimica Acta 51 (2006) 1473-1479. https://doi.org/10.1016/j.electacta.2005.02.128
[51] P. Zoltowski, On the electrical capacitance of interfaces exhibiting constant phase element behaviour, Journal of Electroanalytical Chemistry 443 (1998) 149-154. https://doi.org/10.1016/S0022-0728(97)00490-7
[52] G. Grundmeier, W. Schmidt, M. Stratmann, Corrosion protection by organic coatings: electrochemical mechanism and novel methods of investigation, Electrochimica Acta 45 (2000) 2515-2533. https://doi.org/10.1016/S0013-4686(00)00348-0
[53] T. Matsuda, K.B. Kashi, K. Fushimi, V.J. Gelling, Corrosion protection of epoxy coating with pH sensitive microcapsules encapsulating cerium nitrate, Corrosion Science 148 (2019) 188-197. https://doi.org/10.1016/j.corsci.2018.12.012

[54] F. Mansfeld, L.T. Han, C.C. Lee, C. Chen, G. Zhang, H. Xiao, Analysis of electrochemical impedance and noise data for polymer coated metals, Corrosion Science 39 (1997) 255-279. https://doi.org/10.1016/S0010-938X(97)83346-X
[55] M. Kendig, F. Mansfeld, S. Tsai, Determination of the long term corrosion behavior of coated steel with A.C. impedance measurements, Corrosion Science 23 (1983) 317-329. https://doi.org/10.1016/0010-938X(83)90064-1
[56] M. Kendig, S. Jeanjaquet, J. Lumsden, Electrochemical Impedance of Coated Metal Undergoing Loss of Adhesion, in: J. Scully, D. Silverman, M. Kendig (Eds.) Electrochemical Impedance: Analysis and Interpretation, ASTM International, West Conshohocken, PA, 1993, pp. 407–427.
[57] E.D. Kiosidou, A. Karantonis, G.N. Sakalis, D.I. Pantelis, Electrochemical impedance spectroscopy of scribed coated steel after salt spray testing, Corrosion Science 137 (2018) 127-150. https://doi.org/10.1016/j.corsci.2018.03.037
[58] F. Mahdavi, M. Forsyth, M.Y.J. Tan, Techniques for testing and monitoring the cathodic disbondment of organic coatings: An overview of major obstacles and innovations, Prog. Org. Coat. 105 (2017) 163-175. https://doi.org/10.1016/j.porgcoat.2016.11.034
[59] P. Pedeferri, Corrosion Science and Engineering, Springer, Cham, Switzerland, 2018.
[60] C. Compère, É. Fréchette, E. Ghali, The corrosion evaluation of painted and artificially damaged painted steel panels by AC impedance measurements, Corrosion Science 34 (1993) 1259-1274. https://doi.org/10.1016/0010-938X(93)90086-V

Figure 1

Click here to access/download;Figure;Figure 1.tif

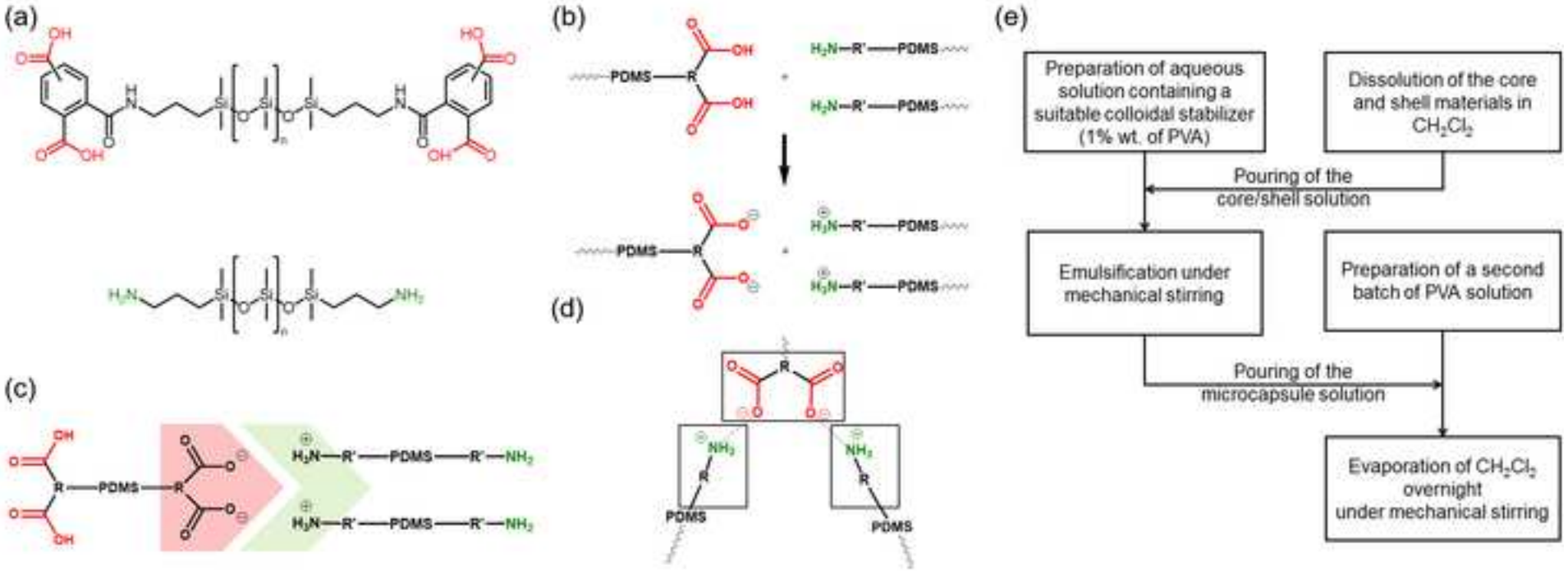

Figure 2

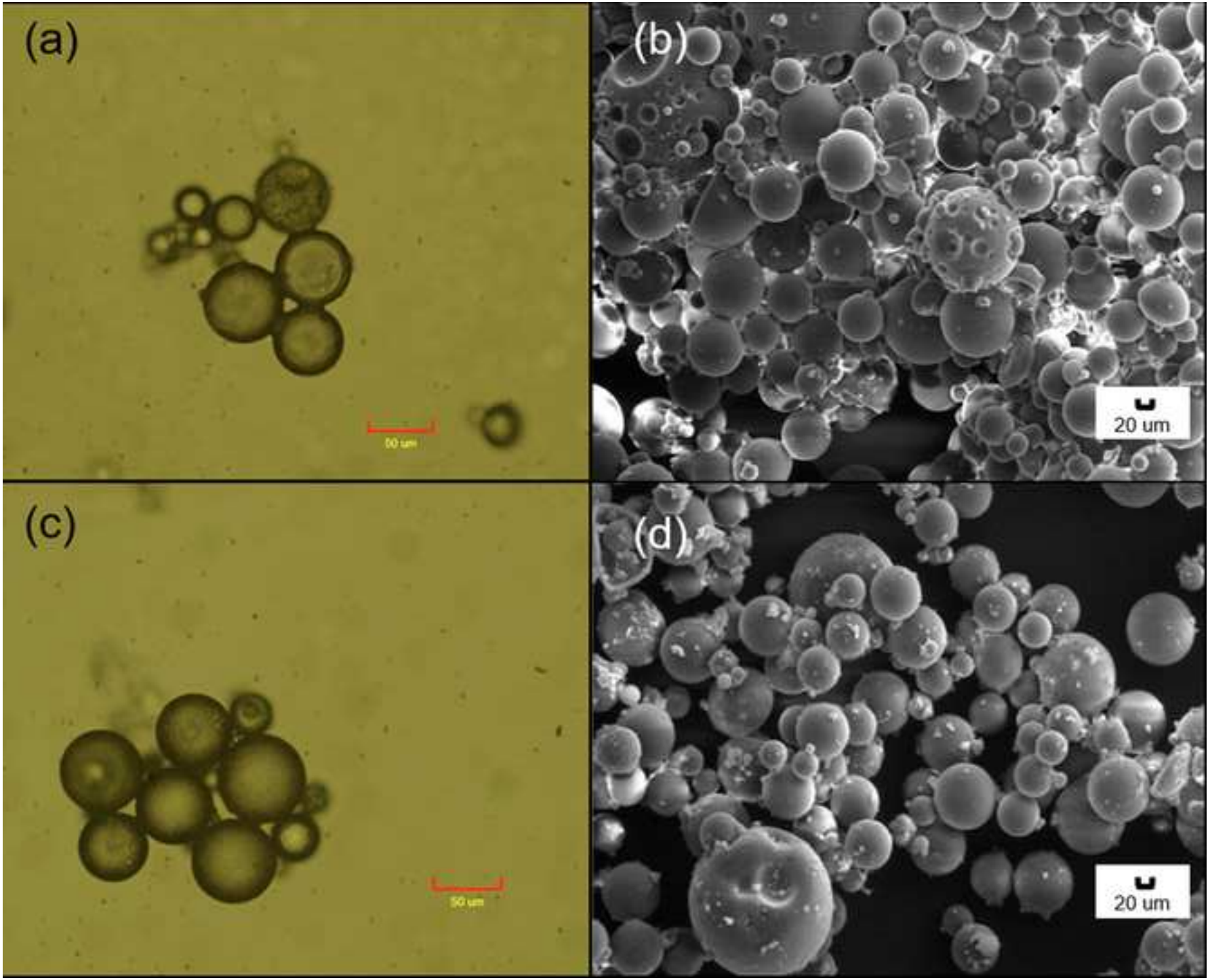

Figure 3

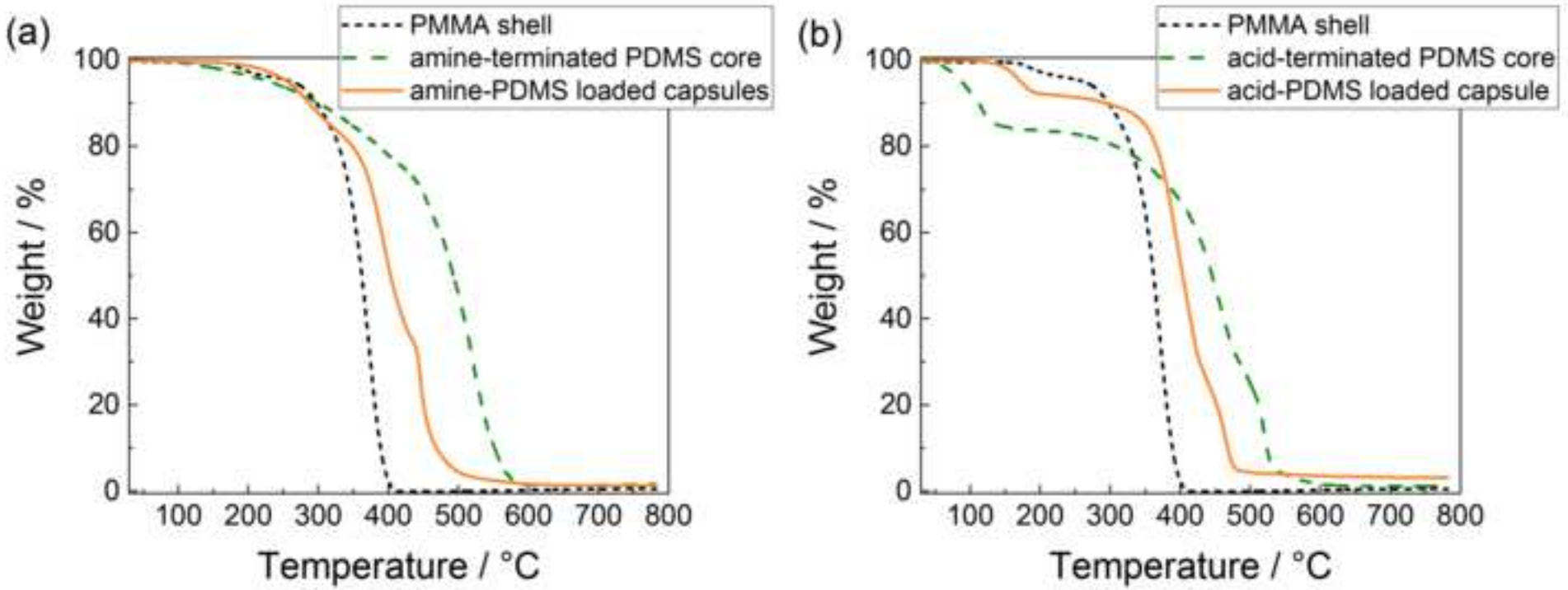

Figure 4

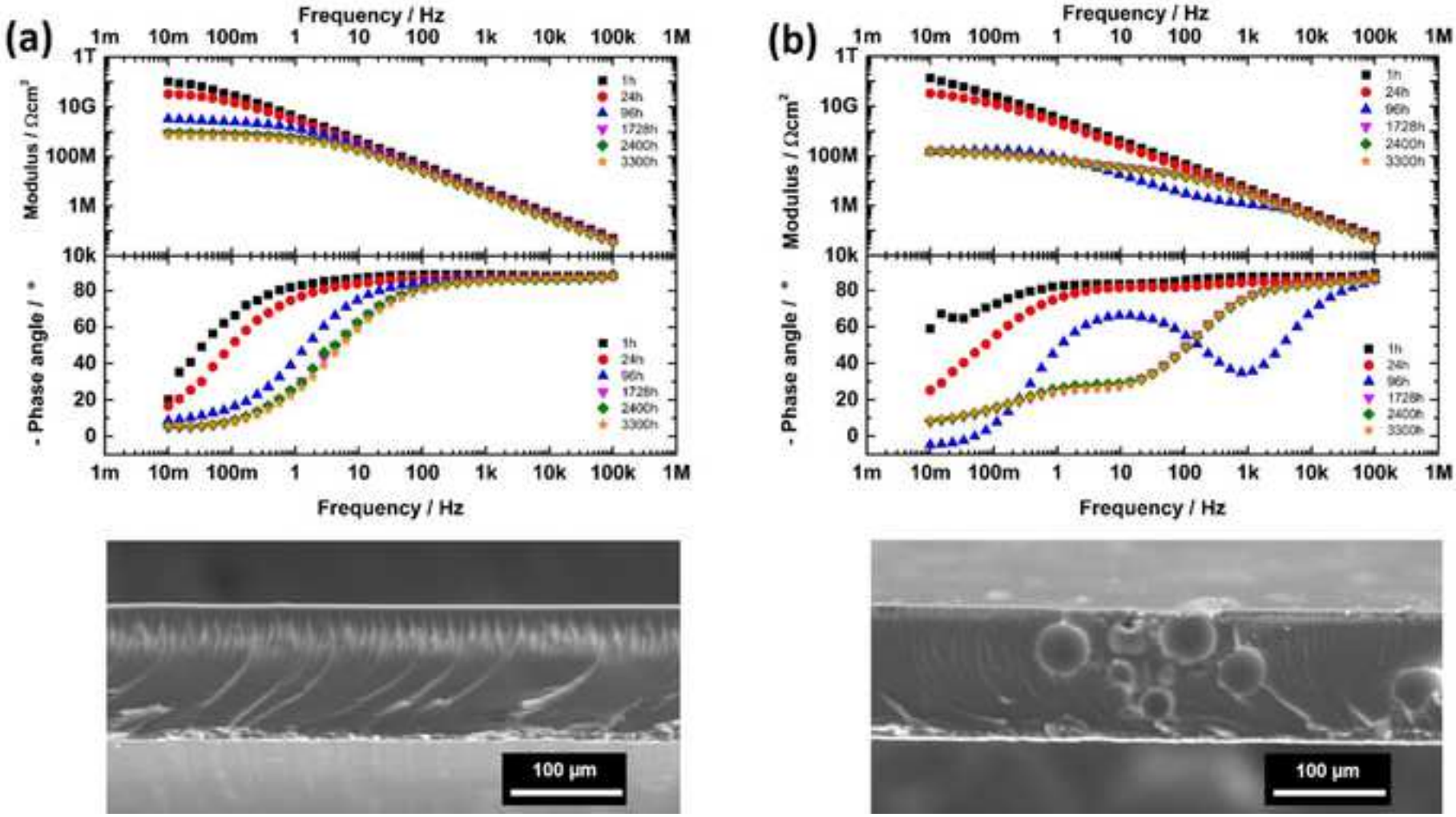

Figure 5

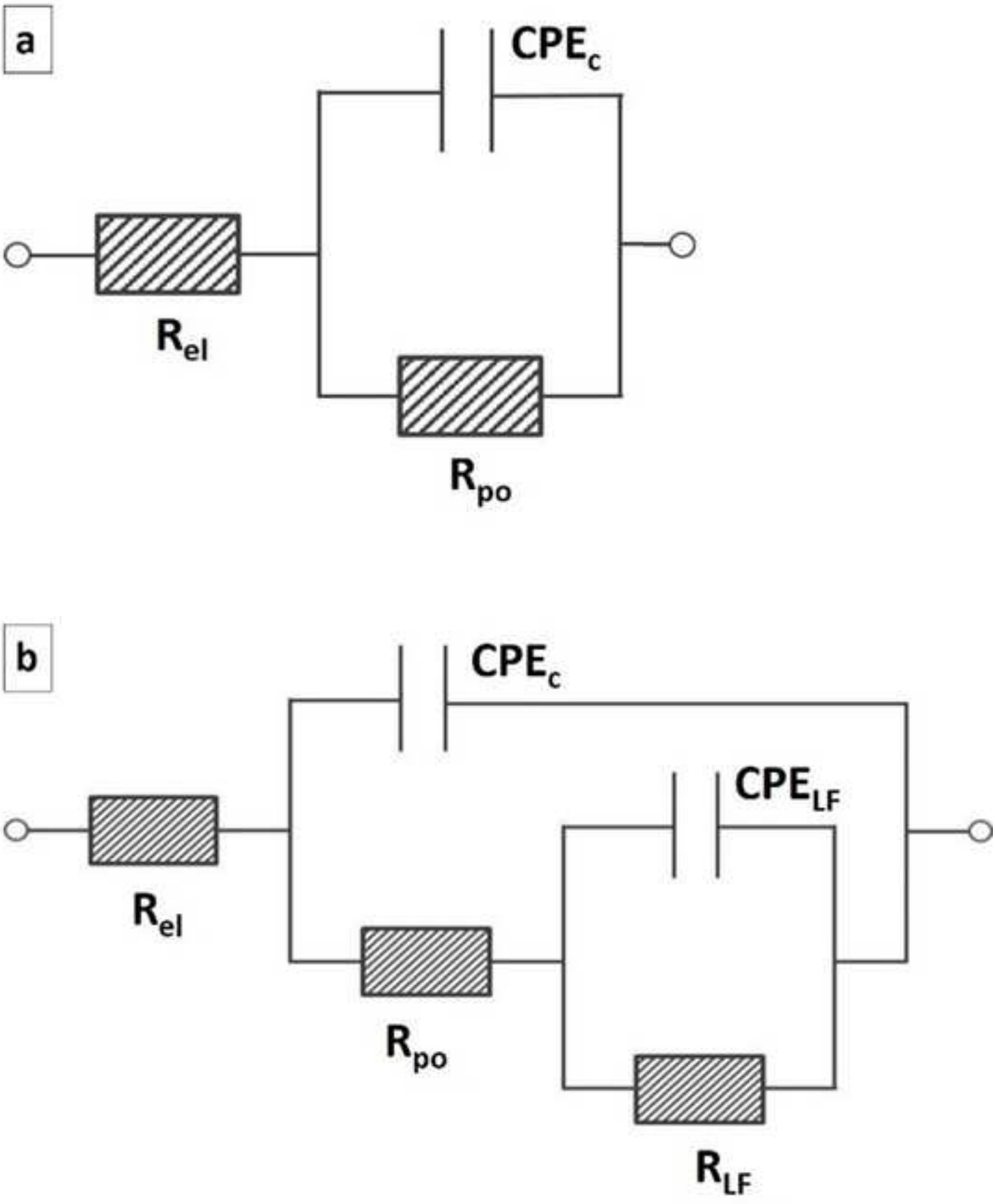

Figure 6

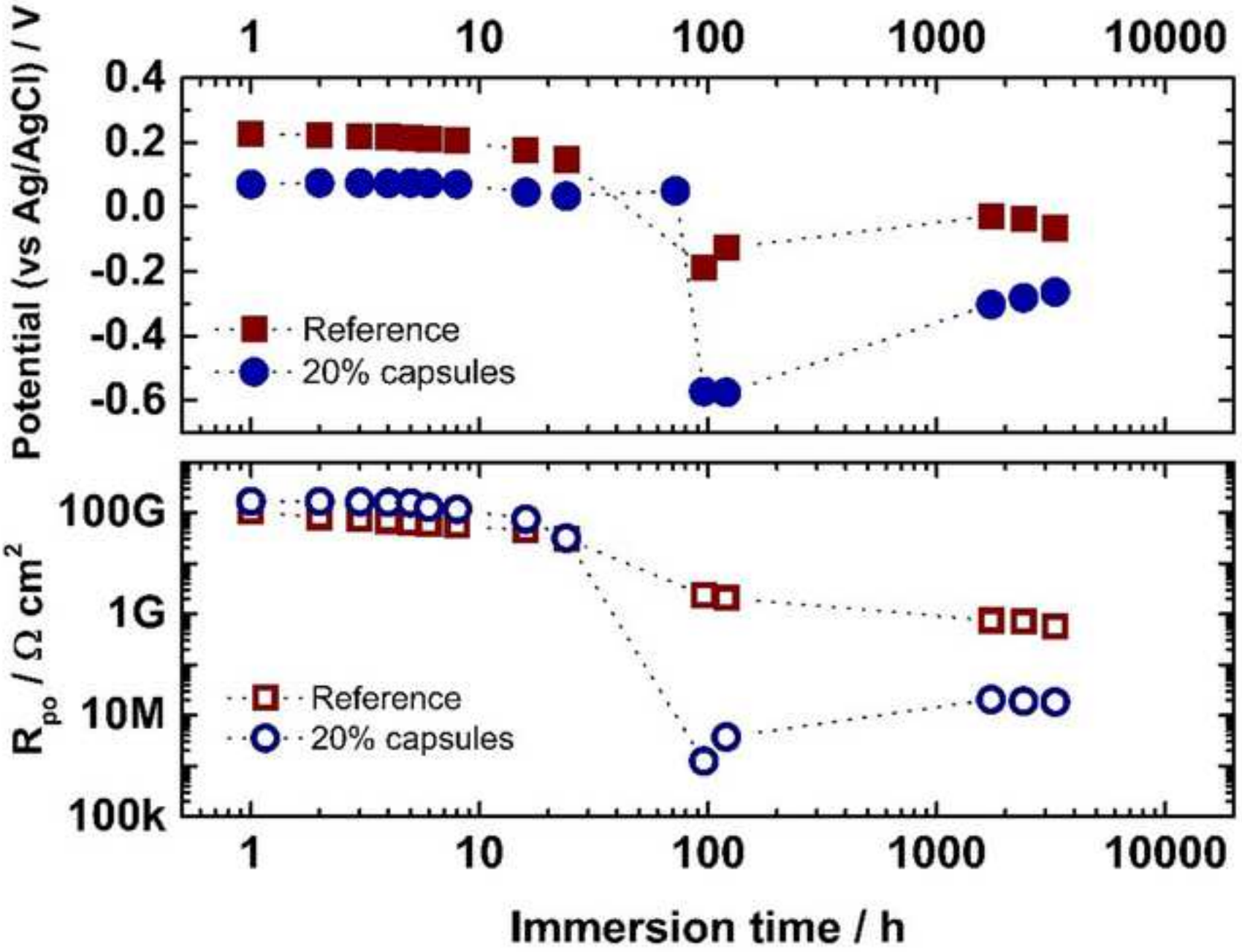

Figure 7

Click here to access/download;Figure;Figure 7.tif

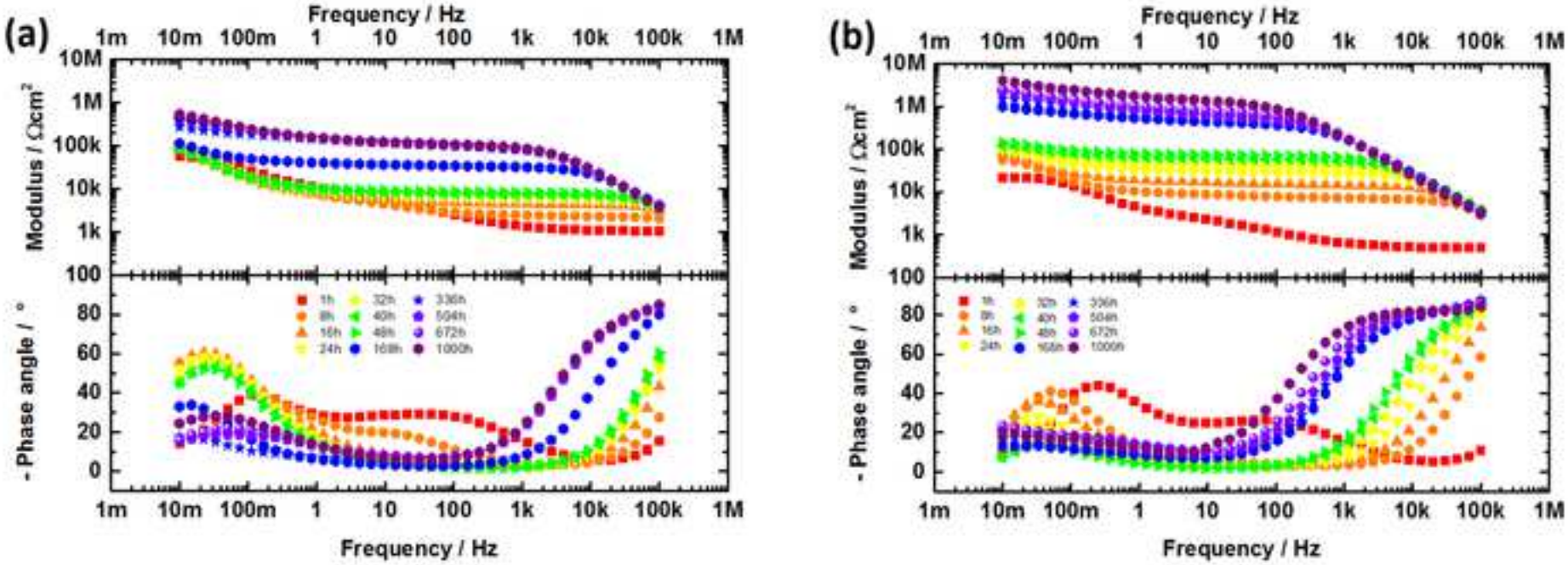

Figure 8

Click here to access/download;Figure;Figure 8.tif

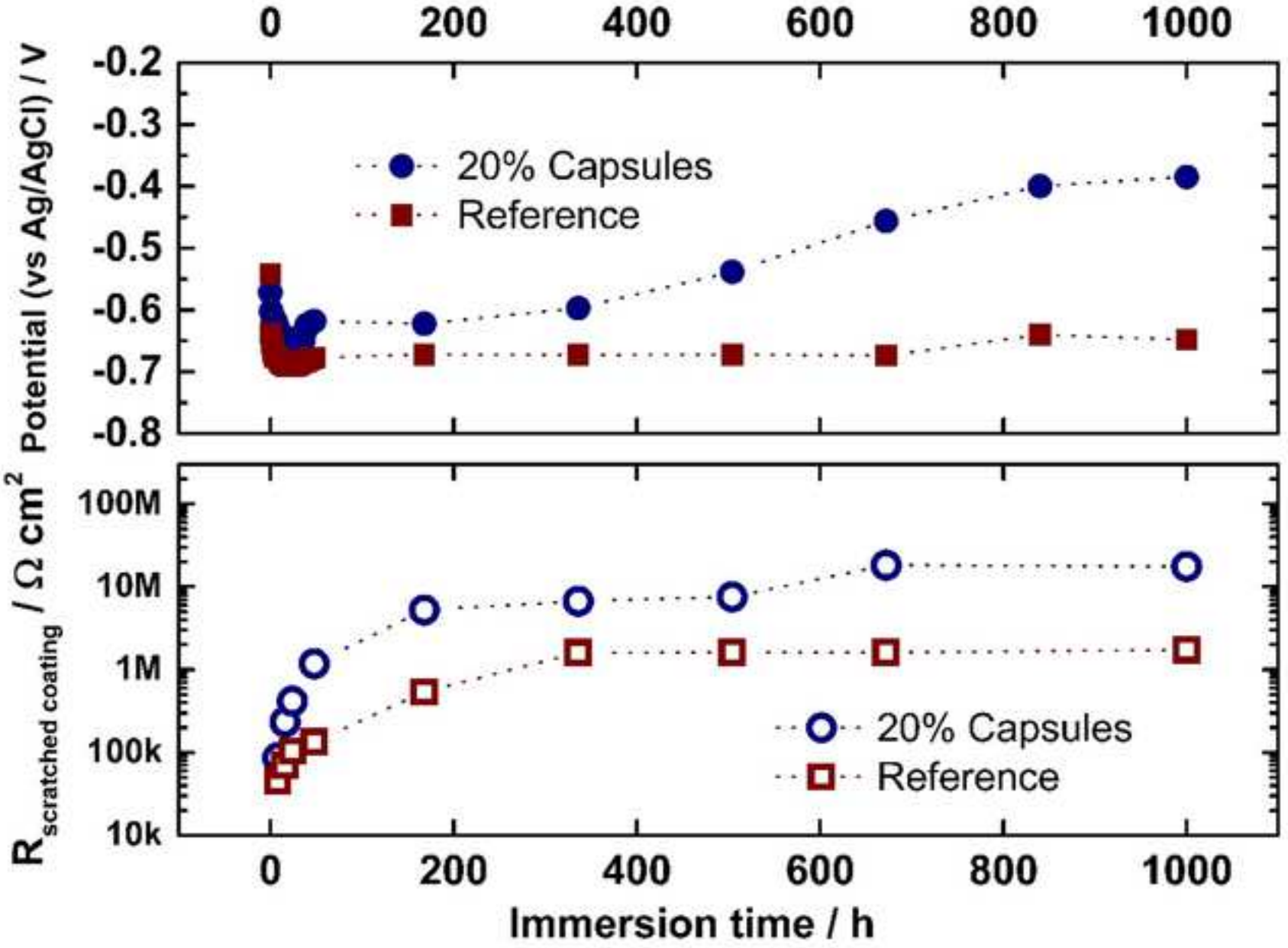

Figure 9

Figure 10

Click here to access/download;Figure;Figure 10.tif